Check for updates

Leaching of phosphate ores with lower dissolution of metallic impurities: the dual role of sodium oleate†

Yuhe Zhou,[a] Guocan Zheng,[ab] Shaodou Cen,[a] Renlong Liu [ORCID] *[ac] and Changyuan Tao[ac]

In this work, we report the use of surfactants to improve the performance of phosphate ore leaching while reducing the concentration of metallic impurities in the leaching solution. Based on the zeta potential analysis, sodium oleate (SOL) is determined as a suitable surfactant because it can change interfacial properties and improve ionic diffusion. This is experimentally demonstrated by the high leaching performance. After that, the reaction conditions on the leaching performance are systematically investigated. Under the optimal experimental conditions (SOL concentration of 10 mg L^{-1}, sulfuric acid concentration of 1.72 mol L^{-1}, leaching temperature of 75 °C, and leaching time of 180 min), a high phosphorus leaching efficiency of 99.51% is achieved. Meanwhile, the leaching solution presents a lower content of metallic impurities. Further measurements performed on the leaching residues indicate that the additive SOL can promote the growth of platy crystals and facilitate PO leaching. Overall, this work demonstrates that the SOL-assisted leaching method allows for highly-efficient utilization of PO and high-purity phosphoric acid production.
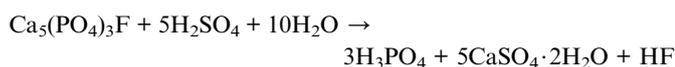
1. Introduction

Phosphoric acid is widely used as an important feedstock for the production of fertilizers, food products, cosmetics, and detergents.[1,2] In 2020, the global phosphoric acid production capacity reached over 58 million metric tons.[3,4] Different approaches such as thermal and wet processes are mainly employed to produce phosphoric acid from phosphate ores (PO).[5,6] The wet process is by far the most common route and the acid can be used in phosphate fertilizer production.[7] In such a hydrometallurgical process, leaching is typically the first step. Sulfuric acid leaching is currently considered the most viable and versatile of the available processes, which is also adopted for the wet process. In the production of wet-process phosphoric acid, PO is reacted with sulfuric acid to produce phosphoric acid and phosphogypsum (PG) *via* the dihydrate process, as described by the reaction below.[8,9]

$$Ca_5(PO_4)_3F + 5H_2SO_4 + 10H_2O \rightarrow$$
$$3H_3PO_4 + 5CaSO_4 \cdot 2H_2O + HF$$

[a] *College of Chemistry and Chemical Engineering, Chongqing University, Chongqing 400044, China. E-mail: lrl@cqu.edu.cn*

[b] *Analytical and Testing Center, Chongqing University, Chongqing 400044, China*

[c] *State Key Laboratory of Coal Mine Disaster Dynamics and Control, Chongqing University, Chongqing 400044, China*

† Electronic supplementary information (ESI) available. See DOI: https://doi.org/10.1039/d3ra00897e

However, reserves of high grade PO are depleting due to the extensive utilization, compelling the use of medium and low grade PO.[10] There are a number of approaches to improve the quality of medium and low grade PO, including grinding and classifying,[11] gravity concentration,[12] and flotation.[13] Despite this, the efficient utilization of medium and low grade PO is increasingly important. Different methods have been proposed for the efficient utilization of PO by reducing the loss of phosphorus content, such as advanced oxidation processes,[14] foam control,[8] and organic acid leaching.[15,16] Generally speaking, the leaching performance is efficiently improved by selecting appropriate agents or adopting intensification methods.

Surfactants, consisting of both hydrophilic and lipophilic groups, are oriented on the liquid surface to regulate liquid interfacial properties.[17–19] They have been widely used in the petroleum chemical industry, medicine, and flotation of minerals.[20–22] In mineral leaching processes, surfactants can change interfacial properties and improve ionic diffusion, therefore increasing leaching efficiency.[23–25] For example, Zhang *et al.*[26] enhanced the copper extraction from chalcopyrite using polyoxyethylene nonyl phenyl ether, and the copper concentration in the leaching solution increased from 385.62 to 930.91 mg L^{-1}. Stearyl trimethyl ammonium chloride was used to promote the leaching of nickel from laterite ores, achieving a high efficiency of 94.7% under the optimal conditions.[27] Thus, the utilization of surfactants is an effective way to facilitate mineral leaching.

In addition to the efficient utilization, the dissolution of metallic impurities (*e.g.*, iron, aluminum, and magnesium) from the medium and low grade PO should be carefully considered because such impurities decrease the quality of phosphoric acid.[28,29] The metallic impurities also cause difficulties in downstream purification and sedimentation. For instance, the impurities in the PO affect the size and shape of the PG crystals.[30] The density and viscosity of acid solutions increase as the concentration of dissolved metallic impurities increases.[31,32] Therefore, reducing the impurities in the acid solutions is crucial to improve the quality of phosphoric acid and facilitate downstream purification and sedimentation. Karavasteva[33] studied a set of surfactants on the acid leaching of zinc calcine and found that the concentration of impurities in the solution decreased in the presence of surfactants. This can be attributed to that surfactants selectively form complexes with cationic ions. Thus, the use of surfactants offers a practical way to decrease the content of impurities in leaching solutions.

In this study, to improve the leaching performance and reduce the dissolution of metallic impurities, we use the surfactants as additives to facilitate the extraction of phosphorus from medium-low grade PO. The optimal experimental condition is determined by investigating the effects of surfactant concentration, sulfuric acid concentration, leaching temperature, and leaching time on the overall leaching performance. The produced leaching solution and residue are measured and analyzed using different analytical techniques. Additionally, measurements on the leaching solution (*i.e.*, surface tension and viscosity) and PO (*i.e.*, the variation in the zeta potential) are performed to better understand the leaching mechanism. Computational simulations are conducted to reveal the adsorption interaction energy between SOL particles and PG surfaces and the corresponding preferential adsorption sites.

2. Materials and methods

2.1. Materials and chemicals

The raw PO is provided by Hubei Xingfa Chemicals Group Co., Ltd., China. It is dried at 60 °C and filtered to maintain particles with a diameter of less than 150 μm. Five surfactants are used for the leaching of PO, including sodium dodecylbenzene sulfonate (SDBS), sodium oleate (SOL), cetyl-trimethylammonium bromide (CTAB), polyvinyl pyrrolidone (PVP), and lauryl sulfobetaine (LSB). Details of these surfactants and the sulfuric acid are provided in Table S1.† Deionized water is produced by a water purification system (HMC-WS10, Human Corporation, Korea).

2.2. Experiments

2.2.1. Acid leaching. The acid leaching of PO is performed at a constant temperature by mixing certain amounts of deionized water, PO, surfactant, and sulfuric acid (*cf.* Fig. S1 of ESI†). After the reaction, the leaching solution and residue are separately obtained using a membrane filter (0.22 μm pore size).

Subsequently, the leaching solution is analyzed to quantify the leaching efficiency of phosphorus with eqn (1).

$$\eta_{\mathrm{p}} = \frac{C_{\mathrm{p}} V_{\mathrm{l}}}{m_{\mathrm{PO}} M_{\mathrm{P}}} \quad (1)$$

where C_{p} is the concentration of phosphorus in the leaching solution (g mL^{-1}), V_{l} is the volume of the leaching solution (mL), m_{PO} is the weight of PO (g), and M_{P} is the grade of PO (wt%). On the other hand, after being dried at 60 °C for 24 h, the leaching residue is further analyzed.

2.2.2. Sedimentation of leaching solution. The leaching solution is subsequently preserved at 25 °C. After that, the sediment (*i.e.*, sludge) and acid solution are obtained *via* centrifugation separation separately. Further analyses are performed on the acid solution and sludge that is washed with deionized water and dried at 60 °C for 24 h. The amount of sludge η_{s} is calculated with eqn (2).

$$\eta_{\mathrm{s}} = m_{\mathrm{s}}/V_{\mathrm{l}} \quad (2)$$

where m_{s} is the weight of obtained sludge and V_{l} is the volume of the leaching solution.

2.3. Analytical techniques

PO samples and leaching residues are analyzed by an X-ray diffractometer (XRD-6000, Shimadzu Corporation, Japan) using Cu Kα radiation as the X-ray source ($2\theta = 5$–$90°$), an X-ray fluorescence (XRF) spectrometer (XRF-1800, Shimadzu Corporation, Japan), and a scanning electron microscopy (SEM) (Quattro S, Thermo Fisher Scientific, US) equipped with an energy dispersive spectroscopy (EDS). The concentration of phosphorus is determined by a UV-Visible (UV-vis) spectrophotometer (722S, Lengguang Tech., China) using ammonium molybdate as the reagent. The concentration of metal ions is determined *via* an inductively coupled plasma optical emission spectroscopy (ICP-OES) (SPECTROGREEN, SPECTRO Analytical Instruments, Germany). The size and shape of leaching residue particles are analyzed by a dynamic image analyzer (QICPIC/L02-OM, Sympatec, Germany). The surface tension of the solutions is analyzed by a surface tension apparatus (JK99C, POW-EREACH, China). The zeta potentials of PO and leaching residues are measured by dynamic light scattering (NanoBrook Omni, Brookhaven Instruments, UK). The viscosity of the leaching solution is measured by a digital rotational viscometer (SNB-2, Jingtian, China).

3. Results and discussion

3.1. Characterization of PO samples

Table 1 tabulates the elemental composition of PO analyzed by the XRF spectrometer. The PO samples mainly contain CaO, P_2O_5, SiO_2, and Al_2O_3 with mass fractions of 45.79%, 31.69%, 11.39%, and 3.24%, respectively. This can also be observed from the SEM-EDS profile in Fig. S2.† In addition, as can be seen from the XRD pattern in Fig. 1, the PO mainly consists of fluorapatite ($Ca_5(PO_4)_3F$) and quartz (SiO_2), along with a small fraction of other mineralogical phases such as glaucophane

Table 1 Elemental composition of PO by XRF

Constituent	CaO	P_2O_5	SiO_2	Al_2O_3	F	MgO
Mass fraction (wt%)	45.79	31.69	11.39	3.24	2.40	1.44
Constituent	K_2O	S	Fe_2O_3	Na_2O	TiO_2	Others
Mass fraction (wt%)	1.23	1.08	0.92	0.35	0.19	0.28
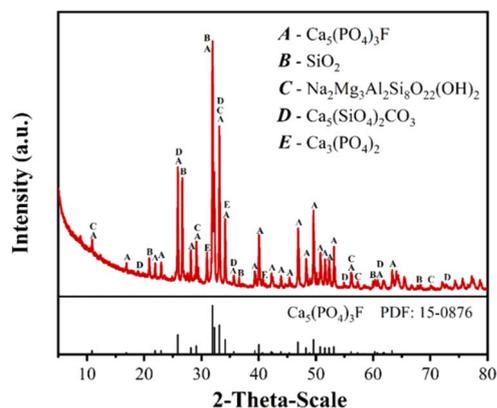
Fig. 1 XRD pattern of PO.

$(Na_2Mg_3Al_2Si_8O_{22}(OH)_2)$, spurrite $(Ca_5(SiO_4)_2CO_3)$, and calcium phosphate $(Ca_3(PO_4)_2)$.

3.2. Zeta potential analysis and surfactant selection

Many researchers have demonstrated that surfactants can modify the interfacial properties of ore particles and improve ionic diffusion, therefore accelerating the reaction.[34,35] Zeta potential is widely used to measure the magnitude of electrostatic repulsion/attraction between particles.[36,37] A high zeta potential (in absolute values) indicates high electrical stability. Fig. 2a compares the zeta potential of PO in different solutions at 25 °C. As a benchmark, the zeta potential of PO in an aqueous solution is −16.35 mV. Higher zeta potentials (in absolute values) are observed for PO in CTAB and SOL solutions, whereas PO in other solutions has relatively low zeta potentials. With a negative zeta potential, PO particles can attract hydrogen ions to accelerate the reaction. Therefore, SOL could be a suitable surfactant for the acid leaching of PO. A preliminary experiment of PO leaching verifies that the SOL is the optimal surfactant due to the corresponding high leaching efficiency (*cf.* Fig. 2b). The experimental results are in good agreement with the previous analysis of zeta potential. The surfactant with a larger negative zeta potential generally has a higher leaching performance. In subsequent experiments, SOL is added to accelerate the acid leaching.

3.3. Optimization of experimental conditions

Different experimental variables (*i.e.*, surfactant concentration, sulfuric acid concentration, leaching temperature, and leaching time) are investigated in this section. Table S2† tabulates the values of experimental variables to be optimized. The leaching without surfactants provides a benchmark against the SOL-assisted leaching, hereinafter referred to as AFR and SOL, respectively.

3.3.1. Surfactant concentration. PO leaching is performed under different SOL concentrations, varying between 0 and 15 mg L^{-1}. The leaching efficiency increases from 87.92% to 98.21% with the SOL concentration rising from 0 to 10 mg L^{-1} (*cf.* Fig. 3a). However, a further increase in the SOL concentration does not improve the leaching efficiency. A possible explanation for this might be that the concentration of SOL exceeds its critical micelle concentration (CMC) and therefore micelles start to form (*cf.* Fig. S3†). Above the CMC, the surface tension of the solution is constant because the concentration of surfactant does not change anymore.[38,39] This will be further explained in Section 3.4. The optimal SOL concentration is set to 10 mg L^{-1} for subsequent experiments.

3.3.2. Sulfuric acid concentration. Fig. 3b shows the effect of the sulfuric acid concentration on the leaching efficiency in the range of 1.12–1.92 mol L^{-1}. The leaching performance of the SOL case is always higher than that of the AFR case. The SOL leaching efficiency increases rapidly and then slightly decreases with the increase of the sulfuric acid concentration. A high acid concentration accelerates the dissolution of PO and therefore improves the leaching efficiency. Whereas an excessive amount of acid increases the viscosity of the leaching solution, hindering the ionic diffusion and PO dissolution. Therefore, the sulfuric acid concentration is set to 1.72 mol L^{-1} in light of the highest leaching efficiency as observed in Fig. 3b.

3.3.3. Leaching temperature. The effect of temperature on the leaching efficiency is studied between 60 and 80 °C. Fig. 3c shows that the leaching efficiency increases with the temperature. A higher temperature facilitates ionic diffusion and therefore leads to better leaching performance. It is also observed that the leaching efficiency of the SOL case is always higher than that of the AFR case. The leaching temperature for subsequent experiments is set to 75 °C because the leaching efficiency is almost constant even if the temperature continues to rise.

3.3.4. Leaching time. The PO leaching is further studied under varying lengths of leaching time as presented in Fig. 3d. The leaching efficiency of the AFR case does not significantly change after the leaching time reached 120 min. Regarding the SOL case, the leaching performance steadily increases with the extension of leaching time. The leaching efficiency reaches the highest value of 99.51% at 180 min, and then slightly drops with extended leaching time. Thus, the leaching time is fixed at 180 min for follow-up investigations.

Based on the experimental data, the statistical significance of experimental variables is analyzed using Design-Expert. All investigated experimental variables are identified as significant terms in the experiments (*cf.* Table S3†), indicating the importance of optimizing experimental conditions. Under the optimal experimental condition, the leaching solution and residue are separately obtained for further investigations.

3.4. Metallic impurities in leaching solution

As mentioned above, a lower concentration of metallic impurities in the leaching solution is crucial to improve the quality of phosphoric acid and facilitate downstream purification and
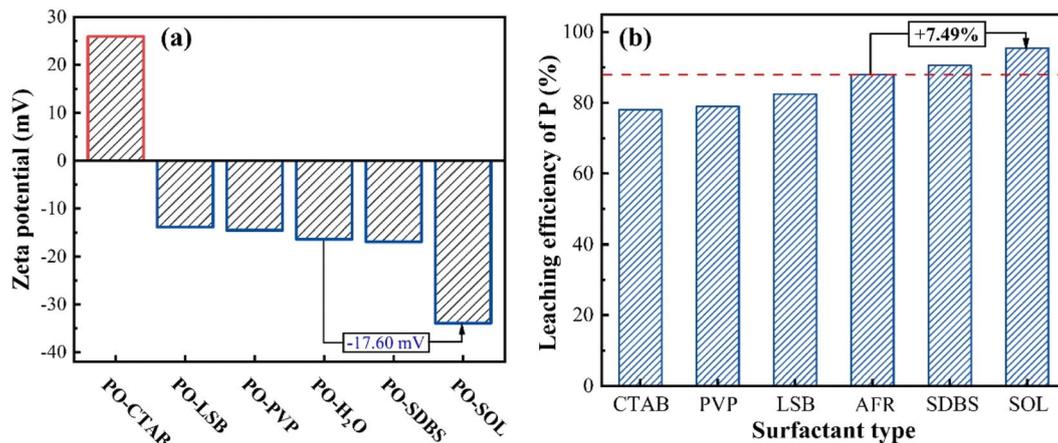
Fig. 2 (a) Zeta potential of PO particles in different solutions and (b) leaching efficiency using different surfactants.

sedimentation. Under the optimal experimental condition, the concentrations of iron, aluminum, and magnesium ions in the leaching solution are measured at different lengths of leaching time. Fig. 4 shows that the concentration of metal ions increases with the extension of leaching time. This is easy to understand. The SOL case presents a reduced amount of Mg, Al, and Fe ions in the leaching solution. This indicates that the

addition of SOL mitigates the dissolution of metallic impurities from PO. A likely explanation is that metallic impurities and SOL are co-sedimented during the PO leaching.

3.5. Sedimentation of leaching solution

The sediment (*i.e.*, sludge) and acid solution are separately obtained after the sedimentation of the leaching solution. The
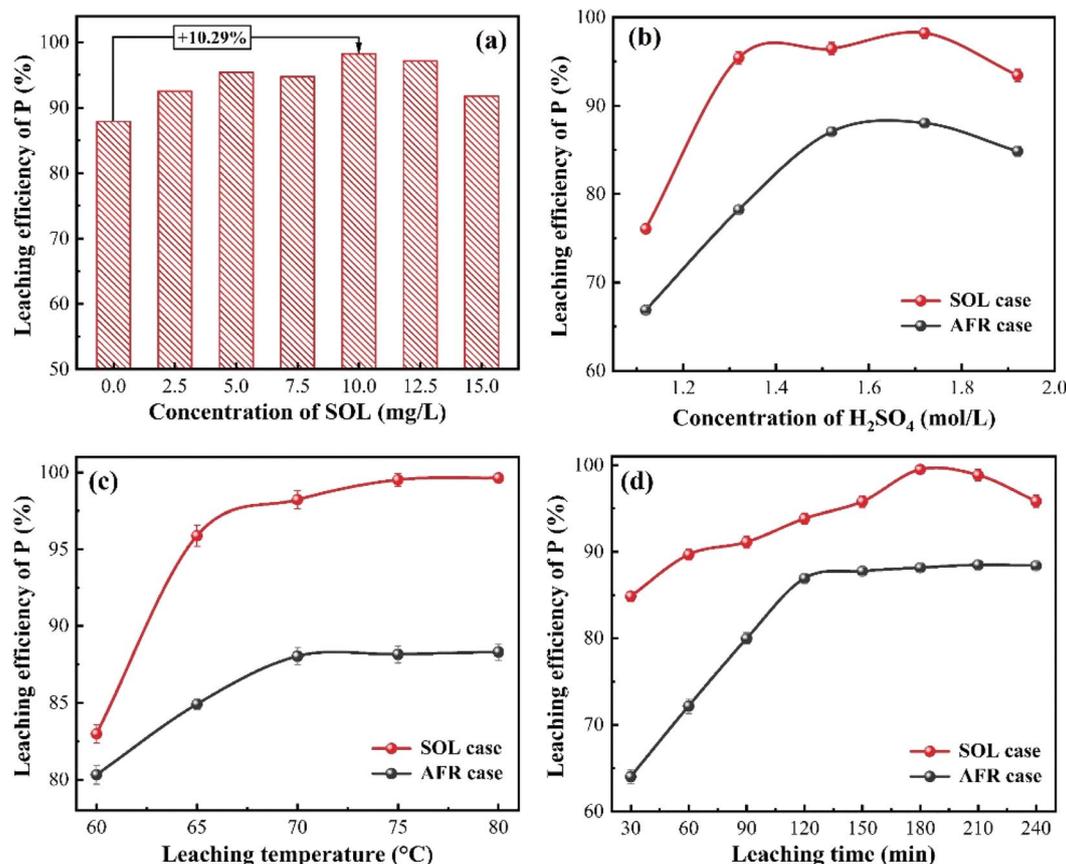
Fig. 3 Leaching efficiency under different (a) SOL concentrations, (b) sulfuric acid concentrations, (c) leaching temperatures, and (d) lengths of leaching time.
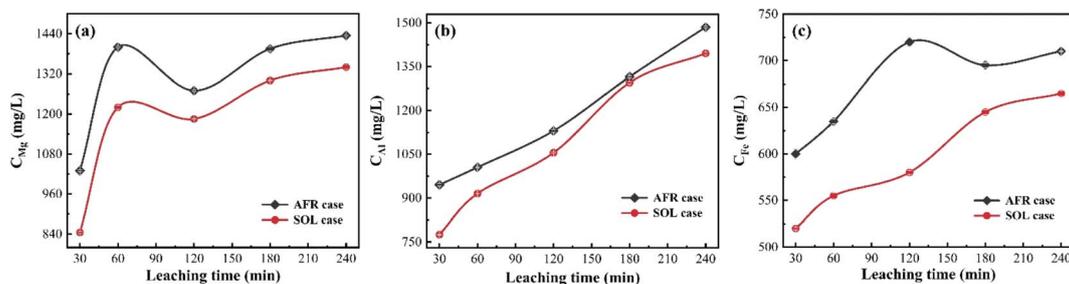
Fig. 4 Concentration of metallic impurities including (a) magnesium, (b) aluminum, and (c) iron ions in the leaching solution.
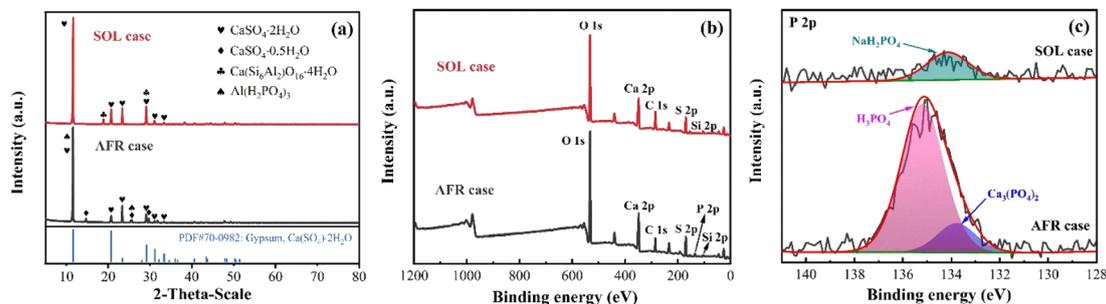

Fig. 5 (a) XRD patterns of the sludge samples, (b) overall XPS spectra of the sludge samples, and (c) deconvoluted XPS spectra for P 2p.

amount of sludge in the SOL case is generally lower than that of the AFR case (*cf.* Fig. S4†). The main phases of the sludge in different leaching cases are measured by the XRD (*cf.* Fig. 5a). In the AFR case, the main compositions of sludge are $CaSO_4 \cdot 2H_2O$, $CaSO_4 \cdot 0.5H_2O$, and $Al(H_2PO_4)_3$. For the SOL case, the

main components of the sludge are $CaSO_4 \cdot 2H_2O$ and $Ca(Si_6Al_2)O_{16} \cdot 4H_2O$. The X-ray photoelectron spectroscopy spectra (XPS) in Fig. 5b, c and S5† are used to better interpret the compositions of the sludge samples, for both AFR and SOL cases (with the corresponding XPS data tabulated in Table S4†). The survey
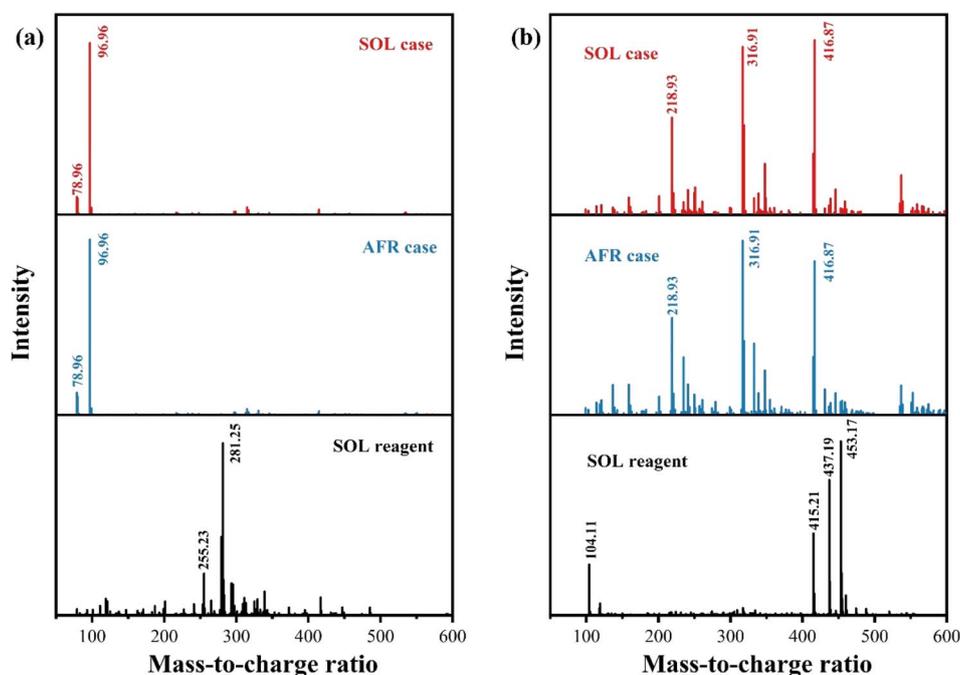

Fig. 6 LCMS analysis of the SOL reagent (purity ≥ 98.5%) and the acid solutions in AFR and SOL cases in (a) negative ion mode and (b) positive ion mode.
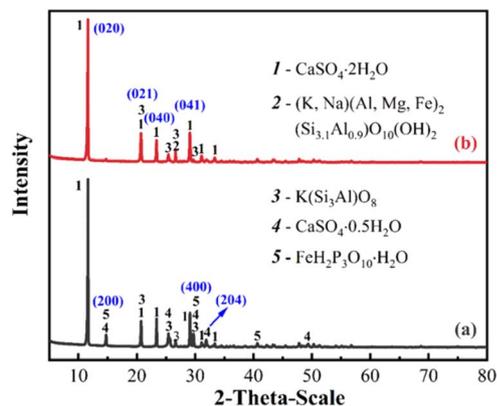
Fig. 7 XRD pattern of the leaching residue for (a) AFR and (b) SOL cases.

spectra in Fig. 5b show the identified characteristic peaks for sludges. A P 2p peak located at 134.9 eV is observed for the AFR case, indicating that a certain amount of phosphorus is sedimented from the leaching solution. The detailed high-resolution P 2p peaks in Fig. 5c show that the amount of phosphorus in the AFR sludge is higher than that in the SOL sludge. This is demonstrated by surface atomic compositions determined by semi-quantitative XPS (presented in Table S5†). The P 2p peak of the AFR sludge can be deconvoluted into two peaks that are assigned to H_3PO_4 and $Ca_3(PO_4)_2$.[40,41] Overall, the addition of SOL can reduce the loss of phosphorus due to the generated sludges.

Furthermore, to examine the presence of SOL, a triple quadrupole mass spectrometer is used to deduce the structure of the compound in the acid solution using both negative and positive ion mode electrospray ionization. Fig. 6a shows that the oleic acid anion $(C_{18}H_{33}O_2^-)$ peaks at 281.25 Da based on the LCMS (liquid chromatography-mass spectrometry) analysis. However, the oleic acid anion is not observed in either AFR or SOL cases. This indicates that no oleic acid anions remain in the acid solution. Additionally, in the positive ion mode, there is no apparent match between the SOL reagent and acid solution (see Fig. 6b). Overall, the SOL is not presented in the acid solution.

3.6. Analysis of leaching residues

The main elemental compositions of the leaching residue are SO_3, CaO, P_2O_5, SiO_2, Al_2O_3, K_2O, Fe_2O_3 and MgO (*cf.* Table S6†). The amount of phosphorus remaining in the residue is 2.02% and 0.50% for AFR and SOL cases, respectively. It demonstrates that the addition of SOL facilitates PO leaching. The XRD pattern in Fig. 7 suggests that the main component of the leaching residue is $CaSO_4 \cdot 2H_2O$ (*i.e.*, PG). The main diffraction peaks at 14.72°, 29.69°, and 31.90° are respectively assigned to (200), (204), and (400) facets of $CaSO_4 \cdot 0.5H_2O$ for the AFR residue.

The morphology of the leaching residue is analyzed by SEM. From Fig. 8a, acicular morphology is observed for the AFR leaching residue. However, for the SOL case, platy structures are mainly observed as shown in Fig. 8b. To further confirm this, the box-counting method is used to analyze the fractal dimension of the leaching residue. The fractal dimension plays a vital
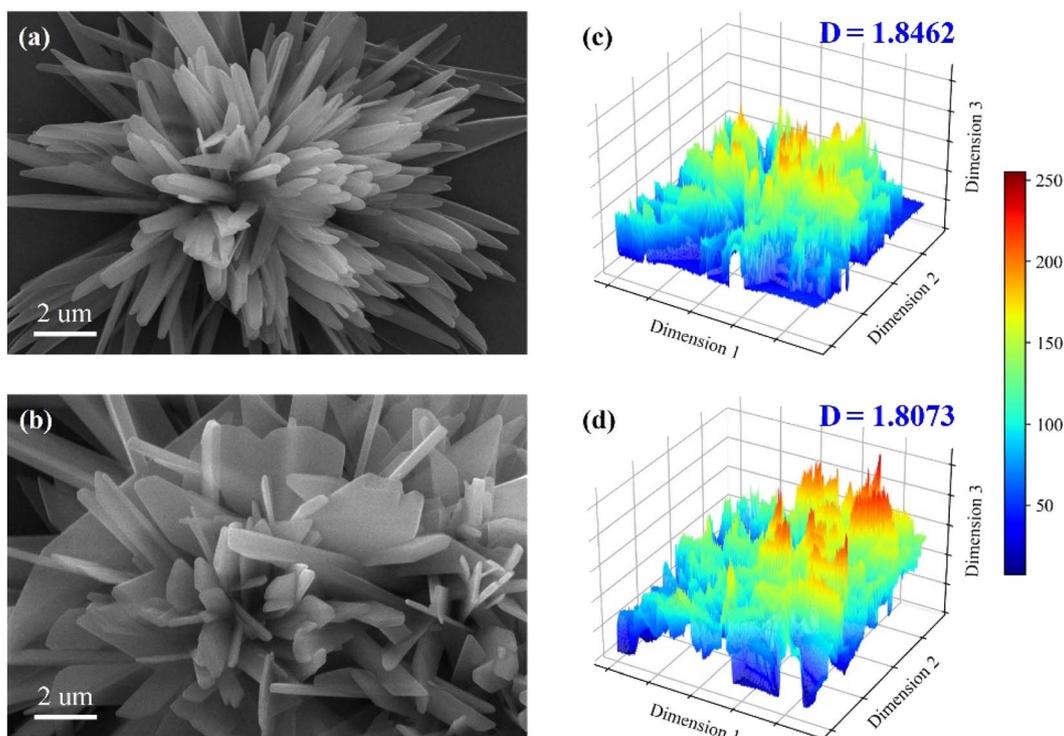

Fig. 8 SEM analysis of the leaching residue in (a) AFR and (b) SOL cases and the analysis of fractal dimension (*D*) for the leaching residue in (c) AFR and (d) SOL cases.
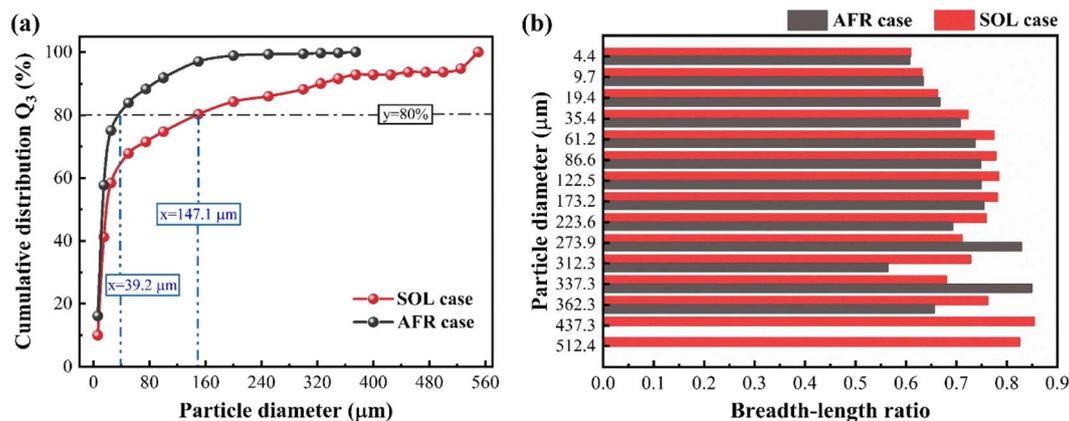
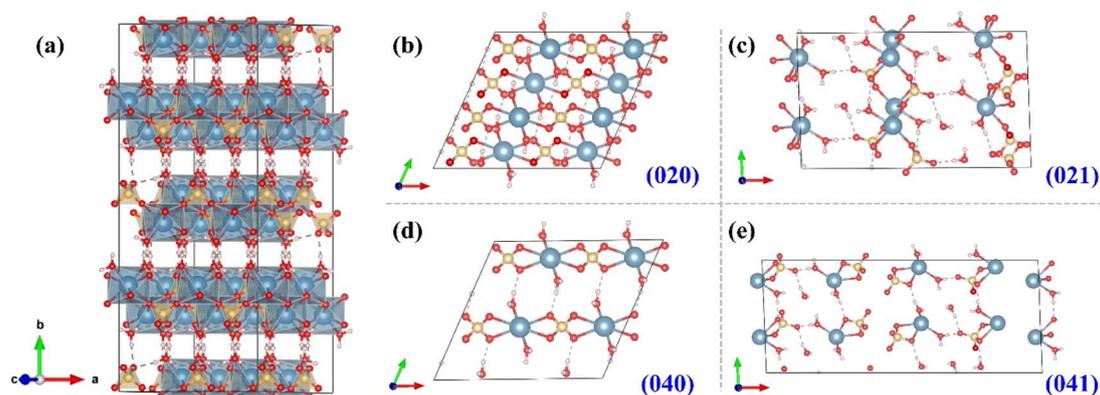Fig. 9 The particle size and shape of the leaching residue.

Fig. 10 Visualization of (a) the unit cell and (b–e) (020), (021), (040), and (041) surfaces of the PG crystal.

role to analyze the complexity of objects.[42–44] A higher fractal dimension indicates higher complexity and irregularity. As shown in Fig. 8c and d, the SOL leaching residue has a lower geometrical complexity for its smaller fractal dimension. SEM images in Fig. S6† show the formation of crystals in the AFR and SOL leaching residues over time, with acicular and platy crystals observed respectively.

Additionally, we compare particle size and shape of leaching residues using the particle analyzer QICPIC. Fig. 9a shows that the particles of the SOL leaching residue have larger diameters and over 80% of particles have a diameter larger than 147.1 μm. This indicates that more uniform, large, and platy crystals are formed during the SOL-assisted PO leaching. Fig. 9b provides a comparison of the breadth-to-length ratio of leaching residues. The crystal of SOL leaching residues mainly has a breadth-to-length ratio between 0.60 and 0.80. This is due to the co-sedimentation of metallic impurities and SOL, facilitating the growth of PG toward large and uniform crystals.

As mentioned above, the main solid product is PG. The adsorption energy between SOL and different PG surfaces is calculated based on density functional theory (DFT). The optimization of unit cells of crystals and molecules is performed using Materials Studio. The DMol3 module is used to simulate

the molecular dynamics of the SOL adsorption on the surface of crystals. More details of the DFT calculations can be found in our previous work.[45] Fig. 10 shows the PG crystal structure optimized by Materials Studio, with the structural information of the unit cell tabulated in Table S7.† Fig. 10b–e presents (020), (021), (040), and (041) surfaces of PG crystals, which are also in line with previous reports.[46,47] The adsorption of SOL on surfaces (020), (021), (040), and (041) of $CaSO_4 \cdot 2H_2O$ are visualized in Fig. S7,† and the corresponding adsorption energy is 0.44, −2.33, −1.13, and −6.72 eV, as tabulated in Table 2. A higher binding energy (absolute value) indicates stronger and more favorable adsorption. Therefore, SOL exhibits a stronger chelating ability with the (041) surface of PG. Therefore, the preferential adsorption of SOL on the (041) surface increases

Table 2 Adsorption energy of SOL on different surfaces of the PG crystal. Calculation details are provided in Section S2

Crystal surface	$E_{PG\text{-}SOL}$ (eV)	E_{PG} (eV)	E_{SOL} (eV)	ΔE_{ads} (eV)
(020)	−360 420.86	−332 741.90	−27 679.40	0.44
(021)	−360 414.90	−332 733.19	−27 679.38	−2.33
(040)	−194 049.17	−166 368.62	−27 679.42	−1.13
(041)	−360 393.52	−33 2707.41	−27 679.39	−6.72

the exposure of the (041) surface, promoting the formation of platy PG crystals.

The above investigations on the leaching residue indicate that the SOL inhibits the growth of (200), (400), and (204) surfaces of PG crystals. Platy PG crystals with larger particle sizes and larger breadth-to-length ratios are obtained. SOL promotes the detachment of PG from PO, thereby facilitating the PO leaching and improving the leaching performance.

4. Analysis of enhancement mechanism

Surface tension and viscosity of the leaching solution are measured to explain the effect of SOL on the PO leaching. The addition of surfactant reduced the surface tension of the solution, which increased the wettability of particles and reduced particle–particle interaction.[48] Fig. 11a shows the surface tension of the leaching solution for both AFR and SOL cases, benchmarking against the deionized water. The SOL leaching solution shows a lower surface tension than that of the AFR leaching solution, which allows for improved ionic diffusion and liquid–solid contact. Additionally, the viscosity of the solution also has an important effect on the leaching because

a high solution viscosity hinders mass transfer.[49] Fig. 11b presents the viscosity of the deionized water and the leaching solutions obtained from AFR and SOL cases. The viscosity of the SOL leaching solution is lower than that of the AFR leaching solution, allowing for a higher overall mass transfer coefficient. Therefore, the low surface tension and viscosity could explain the high performance of the SOL-assisted leaching.

Phosphorus in PO mainly exists in the form of fluorapatite ($Ca_5(PO_4)_3F$). To better illustrate the adsorption behavior of SOL on PO, we visualized the fluorapatite crystal structure to showcase its interaction with SOL. A unit cell of fluorapatite (*cf.* Fig. 12a) is constructed based on the structural information obtained from the American Mineralogist Crystal Structure Database[50] (tabulated in Table S8†). The (001) surface of fluorapatite crystals is used to illustrate the interaction because it is the most exposed and stable (*i.e.*, with the lowest surface energy).[51,52] SOL is a common anionic surfactant, whose polar group presents electronegative.[53] When SOL is added into the system, the polar group is adsorbed on the fluorapatite surface and the nonpolar group is oriented towards leaching solution externally, as shown in Fig. 12b. The PO particles will be in a stable dispersion state due to the electrostatic repulsion, which also contributes to the contact between the PO surface and the leaching solution. Thus, such interactions between SOL and PO would promote the dissolution of PO and therefore improve the leaching efficiency.
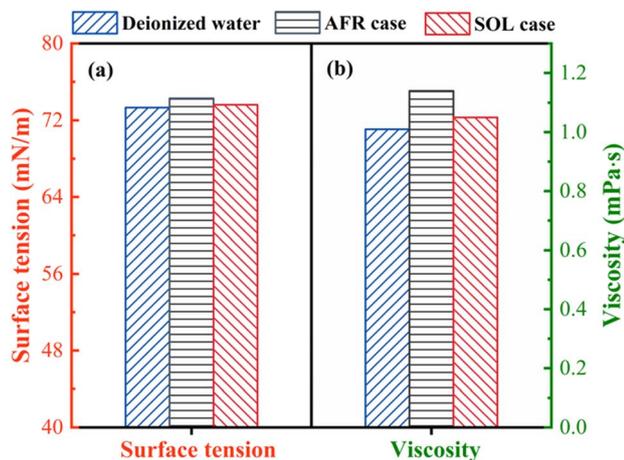
5. Conclusion

This study adopted SOL as an additive to investigate its performance in facilitating PO leaching. The SOL is determined as a suitable surfactant based on the zeta potential analysis. Under the optimal experimental condition (SOL concentration of 10 mg L^{-1}, sulfuric acid concentration of 1.72 mol L^{-1}, leaching temperature of 75 °C, and leaching time of 180 min), a high leaching efficiency of 99.51% is achieved. It is 12.89% higher than the leaching without the addition of SOL. In addition, SOL-assisted leaching presents a lower concentration of metallic impurities in the leaching solution. This increases the quality of phosphoric acid and could promote downstream purification and sedimentation. The low surface tension and viscosity of the leaching solution are beneficial for ionic
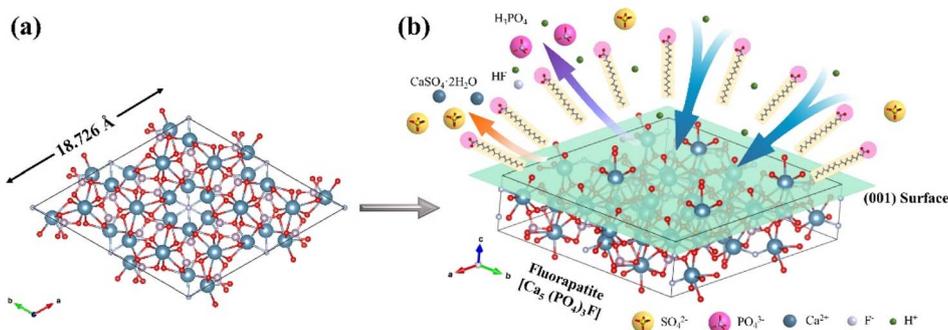

Fig. 11 Surface tension and viscosity of leaching solutions.

Fig. 12 Visualization of (a) the fluorapatite crystal and (b) the adsorption of SOL on the PO surface.

diffusion and liquid–solid contact, therefore leading to the high performance of SOL-assisted leaching. The DFT-based calculation indicates that SOL is preferentially adsorbed on the (041) surface of PG crystals, tuning the PG morphology from the acicular shape to the platy shape. Overall, this study demonstrates the advantages of SOL in improving the leaching performance and reducing the metallic impurities in the leaching solution, enabling the high-efficient utilization of PO and the production of high-purity phosphoric acid.

Despite that a lower content of metallic impurities is achieved, it is still insufficient for subsequent nucleation and crystallization to produce high-quality products. Thus, a further investigation of thorough removal of metallic impurities is necessary to ensure the quality of the final products. Additionally, from the perspective of industrial production, a huge amount of sludge will be produced, which deserves further investigation. Therefore, the recovery and utilization of the deposited sludge could also be an interesting and meaningful topic for future work. Moreover, further research in the study of crystallization kinetics would be of great help in understanding the mechanism of crystal growth and for controlling the crystal shape.

Author contributions

Yuhe Zhou: investigation, conceptualization, formal analysis, writing – original draft. Guocan Zheng: resources, funding acquisition. Shaodou Cen: software. Renlong Liu: supervision, project administration, funding acquisition, writing – review & editing. Changyuan Tao: supervision.

Conflicts of interest

There are no conflicts to declare.

Acknowledgements

References

1 H. Zhuang, Y. Zhong and L. Yang, *Chin. J. Chem. Eng.*, 2020, **28**, 2758–2770.

2 S. Pavón, N. Haneklaus, K. Meerbach and M. Bertau, *Miner. Eng.*, 2022, **182**, 107569.

3 Statista, 2022, **https://www.statista.com/statistics/1289304/global-phosphoric-acid-production-capacity/**.

4 Z. Ren, W. Zeng, H. Liu, Y. Jia, X. Peng and Y. Peng, *Process Saf. Environ. Prot.*, 2021, **156**, 121–133.

5 P. Becker, *Phosphates and phosphoric acid: raw materials, technology, and economics of the wet process. revised and expanded*, Marcel Dekker, Inc., 1989.

6 H. Ma, X. Feng and B. Zeng, *Process Saf. Environ. Prot.*, 2018, **118**, 330–347.

7 H. Tayibi, M. Choura, F. A. Lopez, F. J. Alguacil and A. Lopez-Delgado, *J. Environ. Manage.*, 2009, **90**, 2377–2386.

8 H. Li, W. Ge, J. Zhang, R. M. Kasomo, J. Leng, X. Weng, Q. Chen, Q. Gao, S. Song, L. Xiao and C. Tian, *Hydrometallurgy*, 2020, **195**, 105364.

9 B. Ji, Q. Li, Q. Huang and W. Zhang, *J. Cleaner Prod.*, 2021, **319**, 128654.

10 X. Shao, H. Yao, S. Cui, Y. Peng, X. Gao, C. Yuan, X. Chen, Y. Hu and X. Mao, *Sci. Total Environ.*, 2021, **780**, 146550.

11 A. Z. Abouzeid, *Int. J. Miner. Process.*, 2008, **85**, 59–84.

12 B. Issa and T. A. Aleksandrova, *IOP Conf. Ser.: Mater. Sci. Eng.*, 2019, **582**, 012022.

13 T. Aleksandrova, A. Elbendari and N. Nikolaeva, *Miner. Process. Extr. Metall. Rev.*, 2022, **43**, 22–27.

14 Y. Zhou, G. Zheng, Y. Long, Z. Liu, C. Tao and R. Liu, *Hydrometallurgy*, 2022, **210**, 105842.

15 D. E. Lazo, L. G. Dyer and R. D. Alorro, *Miner. Eng.*, 2017, **100**, 115–123.

16 M. Gharabaghi, M. Irannajad and M. Noaparast, *Hydrometallurgy*, 2010, **103**, 96–107.

17 B. Li, H. Peng and J. Guo, *Appl. Sci.*, 2019, **9**, 1684.

18 Z. Lin, F. Xu, L. Wang, L. Hu, L. Zhu, J. Tan, Z. Li and T. Zhang, *Chin. J. Chem. Eng.*, 2021, **34**, 53–60.

19 M. Clotilde Apua and M. S. Madiba, *J. Taiwan Inst. Chem. Eng.*, 2021, **121**, 313–320.

20 C. Liu, S. Liu, Y. Qin, J. Ma, Z. Wu, J. Zhou, R. Lyu and C. Wang, *Sep. Purif. Technol.*, 2019, **212**, 89–100.

21 W. Pan, H. Jin, Z. Liu, J. Tang and S. Cheng, *Process Saf. Environ. Prot.*, 2020, **137**, 289–299.

22 N. Saxena, N. Pal, S. Dey and A. Mandal, *J. Taiwan Inst. Chem. Eng.*, 2017, **81**, 343–355.

23 P. Zhang, L. Sun, H. Wang, J. Cui and J. Hao, *J. Cleaner Prod.*, 2019, **228**, 1–7.

24 X. Zeng, J. Shu, M. Chen, J. Wang, D. He, Y. Wei, Y. Deng, T. Lei, Z. Liu, D. Tan and Q. Zhang, *Hydrometallurgy*, 2022, **211**, 105870.

25 D. Wu, W. Ma, S. Wen, J. Deng and S. Bai, *Miner. Eng.*, 2017, **114**, 1–7.

26 H. Zhang, D. Wei, W. Liu, D. Hou and R. Zhang, *Miner. Eng.*, 2021, **173**, 107237.

27 P. Zhang, H. Wang, J. Hao and J. Cui, *Front. Chem. Sci. Eng.*, 2021, **15**, 562–570.

28 A. Hannachi, D. Habaili, C. Chtara and A. Ratel, *Sep. Purif. Technol.*, 2007, **55**, 212–216.

29 B. Wang, L. Yang and J. Cao, *ACS Sustainable Chem. Eng.*, 2021, **9**, 14365–14374.

30 W. W. F. Annalize Kruger, Z. Kwela and R. Fowles, *Ind. Eng. Chem. Res.*, 2001, **40**, 1364–1369.

31 M. E. D. W. E. Cate, *J. Chem. Eng. Data*, 1970, **15**, 291–295.

32 H. Abdel-Ghafar, E. Abdel-Aal, M. Ibrahim, H. El-Shall and A. J. H. Ismail, *Hydrometallurgy*, 2019, **184**, 1–8.

33 M. Karavasteva, *Hydrometallurgy*, 2001, **62**, 151–156.

34 J. Yu, Y. Ge, X. Guo and W. Guo, *Sep. Purif. Technol.*, 2016, **161**, 88–95.

35 C. Zhang, P. Li, Y. Cao, H. Hao, W. Peng, D. Teng and G. Fan, *Sep. Purif. Technol.*, 2022, **284**, 120283.

36 D. Al Mahrouqi, J. Vinogradov and M. D. Jackson, *Adv. Colloid Interface Sci.*, 2017, **240**, 60–76.

37 Q. Cao, J. Cheng, S. Wen, C. Li, S. Bai and D. Liu, *Miner. Eng.*, 2015, **78**, 114–121.

38 Z. Sakhaei and M. Riazi, *Process Saf. Environ. Prot.*, 2022, **161**, 758–770.

39 A. Shadloo, K. Peyvandi and A. Shojaeian, *J. Mol. Liq.*, 2022, **347**, 117971.

40 Y. Barbaux, M. Dekiouk, D. Le Maguer, L. Gengembre, D. Huchette and J. J. A. C. A. G. Grimblot, *Appl. Catal., A*, 1992, **90**, 51–60.

41 S. H. Dittma, *Z. Naturforsch., B: J. Chem. Sci.*, 1974, **29**, 312–317.

42 R. J.-F. Soille Pierre, *J. Visual Commun. Med.*, 1996, **7**, 217–229.

43 X. Yang and M. Wang, *Constr. Build. Mater.*, 2021, **270**, 121376.

44 X. Xing, Z. Zhao and J. Wu, *Chin. J. Chem. Eng.*, 2020, **28**, 466–476.

45 Y. Zhou, S. Wu, R. Liu, Z. Liu and C. Tao, *J. Water Process. Eng.*, 2022, **45**, 102532.

46 X. Sun, G. Zhang and P. Cui, *RSC Adv.*, 2019, **9**, 21601–21607.

47 S. Zhang, H. Qu, Z. Yang, C.-e. Fu, Z. Tian and W. Yang, *Desalination*, 2017, **419**, 152–159.

48 S. Pattanaik, P. K. Parhi, D. Das and A. K. Samal, *J. Taiwan Inst. Chem. Eng.*, 2019, **99**, 193–200.

49 E. Karami, L. Kuhar, A. Bona and A. N. Nikoloski, *Miner. Eng.*, 2021, **170**, 107029.

50 A. Eskanlou, Q. Huang, Y. Foucaud, M. Badawi and A. H. Romero, *Appl. Surf. Sci.*, 2022, **572**, 151499.

51 J. Xie, X. Li, S. Mao, L. Li, B. Ke and Q. Zhang, *Appl. Surf. Sci.*, 2018, **444**, 699–709.

52 P. Rulis, H. Yao, L. Ouyang and W. Y. Ching, *Phys. Rev. B*, 2007, **76**, 245410.

53 Z. Yuan, X. Zhao, Q. Meng, Y. Zhang and Y. Xu, *Miner. Eng.*, 2021, **171**, 107128.